Fibre-Reinforced Shotcrete Test Methods: Impact of the Application Process and Analytical–Numerical Correlations

Todd Clarke[1,2], Peter Schaul[3], Des Vlietstra[4]

[1] : BarChip Inc. Kurashiki, Japan

[2] : Victoria University, Werribee, Australia

[3] : BarChip EMEA Ltd. Dublin, Ireland

[4] : BarChip Australia Pty Ltd. Queensland, Australia

Abstract

Reliable characterization of fibre reinforced concrete (FRC), and particularly fibre reinforced sprayed concrete (FRS - shotcrete), depends on selecting appropriate test methods capable of capturing post-cracking performance and in-situ behaviour. This paper reviews and evaluates key standardised testing approaches, including beam tests, square panel tests and the round determinate panel (RDP) test. Each method provides different insights into toughness, residual strength and crack propagation, and their suitability varies according to whether the specimens are cast or sprayed.

The application process plays a decisive role in the mechanical response. FRS typically exhibits fibre orientation and compaction effects that result in greater strength reductions in flexural beam tests than in cast specimens. In contrast, RDP testing exhibits generally lower reductions in residual capacity for sprayed materials, reflecting its more representative radial cracking pattern and its closer alignment with in-situ behaviour of shotcrete linings. This makes RDP testing particularly relevant for tunnelling and ground-support applications, in which sprayed materials dominate.

A further contribution of this work is to adopt previously developed methodologies that convert RDP load–deflection data into equivalent stress–crack-width (σ–w) behaviour, allowing direct analytical comparison with constitutive curves derived from beam tests. Field test data are used to demonstrate the correlation and highlight the robustness of RDP results for characterising FRS. The findings underscore the importance of test selection and support the effectiveness of RDP testing for realistic assessment of FRS performance and can support numerical modelling using field panel test data. In the paper, an advanced numerical model was prepared for further verification.

Keywords

Synthetic fibre reinforced concrete, FRC, RDP, test methods, verification, FEA

1 Introduction

Fibre reinforced concrete (FRC) is widely used as a structural material because fibres bridge cracks, improve post-cracking behaviour, and increase energy absorption. Depending on fibre type and dosage, this changes the brittle response of plain concrete into strain-softening or strain-hardening behaviour. Accordingly, the fib Model Code 2020 (2024) classifies structural FRC using experimentally determined residual strengths rather than fibre dosage alone.

Fibre reinforced sprayed concrete (FRS) is commonly used for primary ground support in tunnelling and underground construction. Its post-cracking response governs load redistribution, crack control, and serviceability. However, measured performance depends strongly on specimen geometry and test configuration (Parmentier et al., 2008).

FRC is commonly tested using notched beams according to EN 14651 (2005), with residual flexural strengths determined at specified crack mouth opening displacements. Similar procedures are given in ASTM C1609 (2019). Although simple and standardized, beam tests involve a small fracture area and only a limited number of fibres. This can cause significant scatter, particularly at fibre contents below 0.5% by volume (Minelli and Plizzari, 2015). Reported coefficients of variation range from 10% to 30% (Parmentier et al., 2008). This variability may reduce characteristic residual strengths and produce conservative stress-crack width relationships. The single crack plane also does not fully represent the multidirectional stresses in sprayed tunnel linings.

Panel tests better reproduce the structural behaviour of fibre reinforced linings. The Round Determinate Panel (RDP) test, standardized in ASTM C1550 (2020), uses a centrally loaded circular slab supported at three points. Three radial cracks develop, creating a larger fracture area and mobilizing more fibres than beam tests. Consequently, panel tests typically show lower scatter, with coefficients of variation of about 6–9% (Parmentier et al., 2008). Minelli and Plizzari (2015) also found round panels to provide more repeatable post-cracking results.

The RDP test better represents the biaxial stress field and distributed cracking of tunnel linings. Bernard (2002) identified strong correlations between beam and panel results at equivalent crack openings. Minelli and Plizzari (2015) further proposed a method for deriving stress-crack width relationships from panel load-deflection data. This allows panel results to be converted into residual strengths compatible with EN 14651 and the *fib* Model Code 2020 framework.

The distinction between cast FRC and sprayed FRS is also important. Spraying affects fibre orientation and compaction, while beam tests are highly sensitive to the fibres crossing a single crack plane. Preferential alignment parallel to the sprayed surface may therefore reduce measured beam strengths. The radial cracking pattern of the RDP test is less sensitive to fibre orientation, making it particularly suitable for sprayed concrete.

This study compares EN 14651 beam testing with the RDP method for cast and sprayed FRC. Field data are used to evaluate correlation, variability, and robustness. The derived constitutive relationships are then applied in analytical and numerical models. The study highlights the importance of test selection and supports RDP testing as a representative and statistically robust method for sprayed concrete in tunnelling and ground-support applications.

2 Experimental program

The experimental program was designed to evaluate the mechanical performance of two macro synthetic fibre types under both cast and wet mix sprayed conditions, using procedures representative of tunnelling and underground construction practice. The fibres assessed were BarChip 56 which is a fibre 56mm in length and BarChip 48, which is 48 mm in length and served as a benchmark for comparative purposes. Both fibres were tested at dosage rates of 4 kg/m³ and 7 kg/m³.

All sprayed specimens were produced under conditions consistent with site practice. The alkali free accelerator dosage was maintained within the typical project range of 6–8 % by weight of cement. Although it is common in laboratory panel production to reduce accelerator dosage to improve finish and reduce rebound, the program intentionally retained the full in situ dosage. This allowed the study to examine the influence of accelerator content on fibre distribution, early age behaviour, and the comparability between cast and sprayed specimens.

A single concrete mix was developed using locally available aggregates and cementitious materials. The target was to achieve at least 40 MPa compressive strength under sprayed conditions, accounting for the strength reduction typically associated with accelerator use. To ensure this performance margin, a 60 MPa design mix presented below in Table 1 was adopted for all testing.

Table 1: Mix Design of the experimental program for 1 m³ concrete

Constituent	**Amount**		**Constituent**	**Amount**	
Cement	380	kg	Total Batch Water	195	litres
Fly Ash	50	kg	Superplasticiser	~ 4	litres
Silica Fume	20	kg	Retarder	1	litres
Coarse Aggregate 10/7mm	275	kg	Total Weight	2422	kg
Manufactured Sand	1159	kg	Fibre reinforcement	4 and 7	kg
Fine Sand	341	kg			
Slump 200 +/- 20mm,					

Flexural performance was assessed in accordance with EN 14651. Two moulding approaches were used to distinguish between individual-beam effects and bulk cast behaviour. In case of *Individual cast or sprayed beams* the beams were produced directly in single moulds measuring 150 mm × 150 mm × 550 mm. These specimens reflect the influence of mould boundaries, including potential fibre alignment along the walls. While in case of *Cast and cut or sprayed and cut beams* larger beam boxes measuring approximately 1000 mm × 550 mm were used to produce blocks from which six beams were sawn. This configuration reduces the "wall effect", providing a more representative assessment of fibre orientation and distribution in bulk concrete. Test results refer to these categories explicitly to distinguish between boundary affected and boundary free specimens. As part of the test programme, five sprayed RDP specimens, five cast RDP specimens, one cast and one sprayed beam box, and three cast and three sprayed individual beams were prepared for each test series and were cured underwater.

To characterise the influence of accelerator on early age strength, a dedicated core box was sprayed with accelerated concrete. Cores extracted from this box were tested in compression.

In parallel, standard cylinders were cast from the unaccelerated concrete to determine baseline compressive strength for the mix used in casting.

Both cast and sprayed ASTM C1550 round determinate panels were produced to evaluate energy absorption capacity under centrally applied loading, providing an additional performance metric complementary to EN 14651 beam testing.

3 Test results and analytical models

3.1 Standard results

Compressive strength was measured using both cast cylinders (i.e. unaffected by accelerator) and cores extracted from sprayed specimens. Table 2 depicts the 28-day results and illustrates the impact of accelerator on the compressive strength of the 4 mixes.

Table 2: Compressive strength results

Mix	**Dosage [kg/m^3]**	**Cast compressive strength** [MPa] **(CoV)**	**Sprayed compressive strength** [MPa] **(CoV)**	**Reduction due to accelerator** [%]
BC48	4	33.7 (0.9%)	32.2 (27.2%)	4.5
BC48	7	59.5 (2.9%)	46.2 (0.6%)	22.4
BC56	4	59.2 (2.1%)	40.7 (2.8%)	31.3
BC56	7	52.7 (1.1%)	33.8 (1.7%)	35.9

Except for the BC48-4kg sprayed samples (which exhibited low compressive strength in both cast and sprayed specimens), the accelerator significantly reduced the mixes 'compressive strength. This was expected, as highlighted by Galobardes et al (2014), hence why the mix design was developed to produce a 60 MPa shotcrete. As is becoming more common practice in civil shotcrete projects, EN 14651 beam specimens were sprayed and cast as described in section 2.

The results clearly depict a critical difference between sprayed and cast specimens. Through the spraying process, both the impact of accelerator (as seen from the compressive strength results) and fibre alignment can be seen. Second to this, the choice of moulding method also plays a critical role in the outcome. Table 3 shows that spraying or casting individual beams give significantly higher results than spraying or casting larger panels and subsequently sawing beam specimens from these. The walls in the individual moulds create a preferential alignment of the fibres (which would be even more significant for very stiff fibres), and care should be taken if assessing in-situ performance from individual beam results, as the “wall effect” (Juhasz 2020) does not exist in a sprayed tunnel lining, for example. Table 3 highlights the average f_R values and the CoV for each set of beams.

The ASTM C1550 (2020) RDP was used to assess the toughness behaviour of each fibre-reinforced concrete. Engaging a much larger cracked area than the EN 14651 beams, the RDP generally produces sets of results with a significantly lower CoV than that observed from the notched beam test. The impact of spraying on the results can be clearly seen, with significantly lower results observed for sprayed panels compared to cast panels. Table 4 displays the average toughness values for each mix along with the associated CoV for each set of panels.

Table 3: Key results from EN 14651 tests at 28 days age

Set	Mould configuration	Strength LOP f_L [MPa] (CoV)	Strength CMOD1 $f_{R,1}$ [MPa] (CoV)	Strength CMOD2 $f_{R,2}$ [MPa] (CoV)	Strength CMOD3 $f_{R,3}$ [MPa] (CoV)	Strength CMOD4 $f_{R,4}$ [MPa] (CoV)
BC48 4 kg/m^3	Sprayed	4.7 (4.3%)	1.93 (11%)	2.73 (5.6%)	3.03 (11%)	2.73 (11%)
	Cast	7.53 (4.1%)	2.67 (5.7%)	4.1 (2.8%)	4.87 (6.6%)	4.07 (3.8%)
	Sprayed & Cut	3.67 (13%)	1.1 (26%)	1.22 (28%)	1.27 (29%)	1.15 (32%)
	Cast & Cut	5.5 (9.3%)	1.43 (35%)	2.12 (37%)	2.43 (36%)	2.35 (38%)
BC48 7 kg/m^3	Sprayed	4.13 (11%)	2.33 (18%)	3.2 (11%)	3.2 (10%)	3.37 (17%)
	Cast	6.47 (3.6%)	3.5 (10%)	5.53 (9.3%)	6.13 (5.7%)	6.23 (12%)
	Sprayed & Cut	4.2 (15%)	1.68 (57%)	2.42 (56%)	2.55 (53%)	2.45 (53%)
	Cast & Cut	6.65 (5%)	2.72 (19%)	4.45 (18%)	5.28 (14%)	5.2 (16%)
BC56 4 kg/m^3	Sprayed	4.53 (8.4%)	1.77 (32%)	2.57 (29%)	2.8 (27%)	2.8 (23%)
	Cast	6.4 (4.7%)	1.67 (18%)	2.43 (21%)	2.6 (24%)	2.43 (21%)
	Sprayed & Cut	4.5 (7%)	1.3 (11%)	1.77 (18%)	1.93 (17%)	1.83 (21%)
	Cast & Cut	5.1 (4.4%	1.28 (21%)	2.08 (20%)	2.7 (26%)	2.72 (27%)
BC56 7 kg/m^3	Sprayed	4.4 (0 %)	2.1 (8.2%)	3.23 (13%)	3.57 (13%)	3.57 (13%)
	Cast	6.27 (6.6%)	2.83 (7.3%)	4.9 (2%)	5.07 (4.1%)	4.6 (3.8%)
	Sprayed & Cut	3.55 (25%)	1.1 (49%)	1.67 (64%)	1.8 (61%)	1.65 (57%)
	Cast & Cut	5.32 (38%)	2.7 (12%)	3.65 (10%)	3.67 (12%)	3.5 (20%)

Table 4: Key results from ASTM C1550 tests at 28 days age

Set	Mould configuration	Peak Load [kN]	Toughness [J]			
			5 mm	10 mm	20 mm	40 mm
		(CoV)	(CoV)	(CoV)	(CoV)	(CoV)
BC48 4 kg/m^3	Sprayed	23.2 (8.5%)	47.1 (19%)	87 (21%)	145 (19%)	200 (17%)
	Cast	32.9 (4.6%)	73 (6.8%)	145 (9.8%)	254 (11%)	366 (13%)
BC48 7 kg/m^3	Sprayed	25.5 (7.7%)	64 (12%)	135 (13%)	245 (14%)	363 (13%)
	Cast	31.6 (9.5%)	95 (1.6%)	215 (4.4%)	404 (6.2%)	600 (9.7%)
BC56 4 kg/m^3	Sprayed	24.4 (6.1%)	48.9 (3.2%)	96 (5.4%)	170 (6.5%)	257 (6.8%)
	Cast	30.8 (4.7%)	67 (10%)	136 (10%)	237 (10%)	350 (10%)
BC56 7 kg/m^3	Sprayed	24.2 (5.7%)	62 (11%)	134 (8.2%)	241 (2.8%)	356 (5.6%)
	Cast	30.2 (3.9%)	94 (2.4%)	213 (2.9%)	398 (3.5%)	600 (4.4%)

3.2 Derivation of Stress vs. Crack width from RDP's

As the ASTM C1550 test does not include any direct crack width measurement, the derivation of the stress vs. crack width curve requires the estimation of crack width through other means. An alternative to measuring crack width directly is the virtual energy-based yield line method, which derives a simplified crack width relationship from the point load displacement. In this approach, the uniaxial flexural capacity of the material at the point of cracking is combined with an assumed failure pattern to estimate the point load capacity, from which crack width can then be inferred kinematically — without any direct crack measurement (Minelli & Plizzari, 2015).

While the yield line method was originally formulated for nominally plastic materials, meaning its suitability for FRC exhibiting post-crack softening behaviour warrants careful

scrutiny, the experimental validation presented by Minelli & Plizzari (2015) justifies its use fo r this further analysis of RDP results. Equation 1 presents the formula used to convert central deflection to crack width:

$$w = \frac{\sqrt{3}\delta t}{r} \tag{1}$$

where w is the maximum crack width at the bottom of the panel (a function of the crack rotation angle multiplied by the thickness), δ is the post-crack deflection at the centre of the panel (slightly less than the total central deflection at the centre due to elastic deformation of the panel prior to cracking) (Bernard, 2020), t is the average panel thickness, and r is the distance from the centre of the panel to the supports (in this case, 375 mm).

It is suggested by Bernard (2020) that the post-crack flexural strength derived from the RDP is sensitive to panel thickness due to the softening behaviour of FRC, particularly at the larger crack widths. Thinner panels will exhibit a higher flexural strength at a given central deflection than a thicker panel for numerous reasons; however, a modification to the thickness correction factor was proposed by Bernard (2020), to enable a simplified method to be adopted for deriving stress values from the RDP that are independent of thickness. ATSM C1550 includes the following formula for determining the corrected load, P, based on panel thickness and diameter:

$$P = P'\left(\frac{t_o}{t}\right)^{\alpha}\left(\frac{d_o}{d}\right) \tag{3}$$

where P' is the measured load resistance, t_o is the nominal panel thickness (75 mm), t is the measured panel thickness, d_o is the nominal panel diameter (800 mm), d is the measured panel diameter and $\alpha = 2.0 - \delta_c/40$. Bernard proposed a modification to the α factor, which has subsequently been adopted in this work to revise the corrected load for implementation in the derivation of the residual flexural strength from the RDP's. The adopted α factor is:

$$\alpha = 2.0 + \frac{24 - {\delta_c}^2}{30\delta_c} \leq 2 \tag{4}$$

where δ_c is the panel's central deflection as measured by the test method. Based on this, the force value is corrected to account for thickness variations and subsequently, the residual strength values (f_{Ri}) are derived according to Equation (5) (Bernard 2020).

$$f_{Ri} = \frac{2rP}{\sqrt{3}t_o^2 R} \tag{5}$$

where R is the radius of the panel.

3.3 Comparison EN14651 vs ASTM C1550 residual strengths

Residual strengths from both the ASTM C1550 RDP's and the EN 14651 beams have been derived, and the average values are plotted in Figure 1 (a) to (d) for each mix, respectively, as a function of crack width. Using specimens that most closely replicate in situ behaviour, the stress-crack width results derived from the RDP's are compared with the results from the specimens that were sprayed into the large box and sawn into EN 14651 beams. Note that the beam results are plotted as a function of crack width, rather than CMOD, as nominated by the standard, to allow direct comparison with the RDP stress-crack width curves. CMOD is converted to crack width at the tip of the notch using equal triangles (with the assumption that plane sections remain plane). A simplified formula for this conversion is provided in Equation 6 (Minelli & Plizzari, 2015).

$$w_{CTOD} = 0.786 \times CMOD \quad (6)$$

These results show good alignment between the residual strengths derived from the RDP's and those from the EN 14651 beams. The drop after cracking in the RDP is slightly less significant than that observed in the beams, however in majority of cases the two show very similar trends, particularly at ULS (i.e., f_{R3}).

3.4 Constitutive Law

Finally, the ultimate goal of these tests is to extract a constitutive law for the FRC material that can be adopted and applied in design calculations. Based on the test data and the inherent COV in the two test methods, the f_{Ftsd} and f_{Ftud} values have been derived according to *fib* Model Code 2020 (2020) for the BC56 4kg set and compared in Table 5.

Table 5: f_{Ftsd} and f_{Ftud} values

Set	Mould configuration	f_{Ftsd} [MPa]	f_{Ftud} [MPa]
BC56 4 kg/m^3	Sprayed RDP	0.40	0.35
	Cast RDP	0.50	0.47
	Sprayed & Cut Beam	0.31	0.30
	Cast & Cut Beam	0.24	0.32

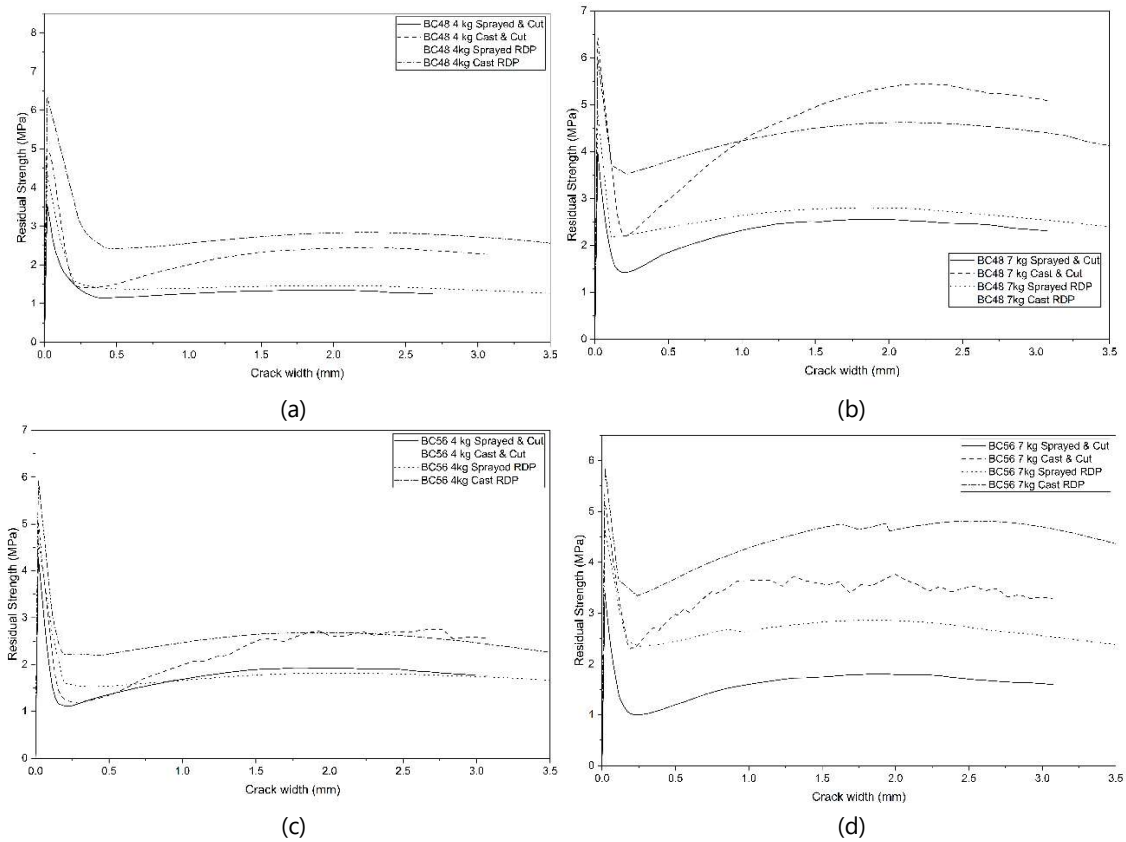


Figure 1: Stress vs crack width derived from both RDP's and sawn beams for (a) BC48 4kg, (b) BC48 7kg, (c) BC56 4kg and (d) BC56 7kg

With the lower scatter of the RDP test and the more representative failure mechanism, the final design values that can be adopted range from 15% to 75% higher than if derived from the beam tests. This difference is significant for design. Because the fib Model Code 2020 derives

characteristic and design values by penalising the mean strength in proportion to its coefficient of variation (CoV), the far greater scatter of the sawn beams (CoV of the residual strengths exceeding 50% for several sprayed-and-cut sets (Table 3)), against markedly lower values for the RDP (Table 4) drives the beam-based design values disproportionately downward. This behaviour is consistent with the wider literature, which reports that the high within-batch variability of beam tests has burdened fibre-reinforced shotcrete design with excessive and uneconomic conservatism (Bernard, 2013; Parmentier et al., 2008), and that characteristic values obtained from small-scale specimens are unrepresentative of, and unduly penalising for, full-scale structures (Cavalaro et al., 2015). Importantly, the higher RDP-derived values are not the result of a relaxed safety format; they follow from reduced test-induced scatter and a failure mechanism that more closely reproduces the in-situ lining. Therefore, they constitute a more reliable, not a less safe, basis for design, provided the adopted partial safety factors continue to reflect the residual tensile strength variability of FRC (Cugat et al., 2020). Adopting the RDP as the reference test thus removes conservatism embedded in the test method rather than in the material, enabling more economical fibre dosages without a corresponding reduction in structural reliability.

While the weight of an RDP can be quite large relative to a beam, the beam box required to produce representative results from sprayed concrete weighs twice as much, at 195 kg. Hence, using RDPs to derive stress crack width results can be a simpler, more efficient method than the currently adopted EN 14651 beams.

4 Numerical inverse analysis

4.1 Material model of concrete and FRC

The concrete was simulated using an advanced constitutive law based on combined failure surfaces. This class of material models enables the representation of the distinct mechanical responses of concrete under tensile and compressive loading, including elastic–plastic and brittle behaviour, compressive and tensile strength limits, and fracture energy dissipation. Various constitutive frameworks have been proposed in the literature for this purpose. The most widely adopted combinations include Von Mises–Rankine, Drucker–Prager–Rankine, and Menétrey–Willam–Rankine criteria, with the Rankine surface typically governing the tensile domain.

It is important to emphasize that these formulations primarily define the peak strength envelope of the material and do not inherently capture the post-cracking softening response. To account for the residual load-carrying capacity after cracking, additional constitutive relationships must be introduced. In the present study, the post-cracking behaviour of fibre-reinforced concrete (FRC) was modelled in accordance with the ITAtech guidelines (ITAtech Activity Group Support, 2015). Crack initiation is assumed to occur when the principal tensile stress exceeds the tensile strength of the concrete. Following crack formation, a residual stress is transmitted across the crack surfaces as a function of crack opening displacement. The stress transfer mechanism is associated with an energy dissipation parameter known as the fracture energy (G_f). This parameter is influenced by aggregate characteristics, including shape (rounded or angular), size distribution, and the quality of the bond between aggregate particles and the cementitious matrix.

The incorporation of fibres increases the fracture energy (G_{Ff}), thereby improving ductility and post-cracking performance. This modelling concept is commonly referred to as the

modified fracture energy approach (Juhász, 2013). In the present numerical models, the enhanced fracture energy was represented by a constant residual tensile strength parameter, f_{Ftu}, calibrated to the specific FRC mix.

Concrete was modelled using three-dimensional solid brick elements and a combined fracture–plasticity constitutive law (Cervenka and Papanikolaou, 2008). Tensile behaviour was represented by a smeared crack and crack band approach with crack initiation governed by the Rankine criterion, while compressive behaviour followed the Menétrey–Willam (1995) failure surface. The uniaxial compressive stress–strain relationship was defined according to Eurocode 2 (Eurocode, 2004), and crack width evolution was derived from the inverse-analysis-based stress–crack opening relationship using the characteristic length concept. This framework enables objective energy dissipation and realistic simulation of crack initiation and propagation in quasi-brittle materials.

4.2 Numerical modelling of the Round Determinate Panel (RDP) test

The numerical validation for BC48 specimens was performed using the finite element software ATENA, a specialized platform for the nonlinear analysis of concrete and reinforced concrete structures developed by Cervenka Consulting (Cervenka et al., 2026). This software enables the implementation of advanced constitutive models suitable for fibre-reinforced concrete, including the combined fracture–plasticity formulation described previously. To ensure accurate replication of the experimental conditions, the complete test configuration was explicitly modelled. This included the loading apparatus and the support conditions.

The analysis was conducted under displacement-controlled loading in order to accurately simulate both the pre-peak and post-peak structural response. Throughout the simulation, midpoint deflection and reaction forces were monitored to obtain the load–displacement relationship.

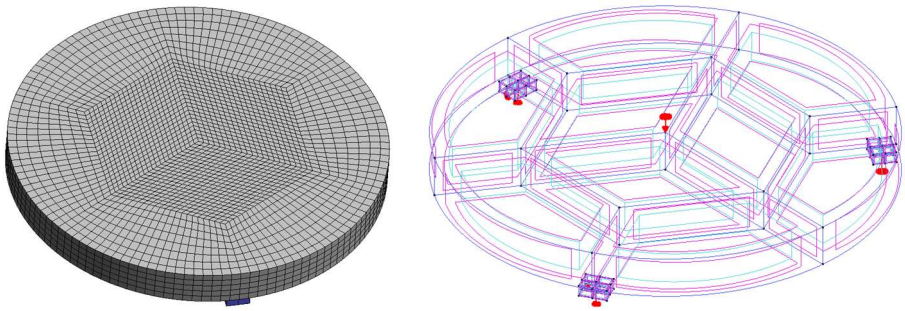


Figure 1: Structural hexahedra mesh of the RDP panel (left), and support - loading conditions (right)

A structured hexahedral mesh (Figure 2) was used to ensure accurate crack localization and propagation. The model was discretized with brick elements of 2.0 cm edge length, with five layers through the thickness to capture stress distribution and damage evolution. The mesh orientation was aligned with the expected crack paths to improve the representation of bending-induced cracking. Support and loading conditions were modelled according to ASTM (2010), with the displacement load applied directly at the centre of the element and without an additional steel distribution plate, enabling close reproduction of the local stress concentrations and boundary conditions of the physical test.

The material parameters were calibrated using the measured mechanical properties obtained from site tests at the age of 28 days. The compressive and tensile strengths were therefore defined on the basis of the real test results. The direct tensile strength was derived from beam test data: first, the flexural tensile strength was determined experimentally, and then the corresponding direct tensile strength was calculated back using the relationship proposed in TR34 (The Concrete Society, 2016). In this way, the input parameters of the constitutive model were linked directly to the measured material response.

The principal objective of the numerical calibration was to adjust the added fracture energy parameter so that the finite element model reproduced the same energy absorption values as those obtained experimentally at deflections of 5, 10, 20, and 40 mm. This criterion was selected because energy absorption is a key performance indicator for fibre-reinforced concrete under flexural loading and provides a robust basis for assessing the adequacy of the post-cracking response predicted by the model. The results of the finite element analysis are presented in Table 6.

Table 6: Mean results of the RDP test and FEA model

Casting method	Dosage (kg/m^3)	Energy absorption of the test [J]				Energy absorption of the FEA [J]			
		5 mm	10mm	20mm	40mm	5 mm	10mm	20mm	40mm
Sprayed	4 kg/m^3	47	87	145	200	52	97	152	224
Cast	4 kg/m^3	73	145	254	366	84	165	262	364
Sprayed	7 kg/m^3	64	135	245	363	82	161	255	356
Cast	7 kg/m^3	95	215	404	600	130	264	462	654

Based on the results, it can be observed that the finite element analysis showed very good agreement with the experimental results at all measured displacement levels for both the sprayed and the cast specimens. This indicates that the calibrated material model was able to capture the structural response with sufficient accuracy not only in the initial loading stage, but also in the post-cracking range characterized by increasing deflection and energy dissipation. The close correspondence between the numerical and experimental energy absorption values confirms that the selected modelling approach, together with the adopted fracture energy calibration procedure, is suitable for reproducing the flexural behaviour of both production technologies.

4.3. The inverse analysis

Inverse analysis is commonly used in the modelling of fibre-reinforced concrete to identify constitutive parameters that cannot be determined directly from standard mechanical tests and must instead be derived by fitting the numerical response to experimental results (Jepsen et al., 2018; Baby et al., 2013). This approach is particularly important for the characterization of the post-cracking tensile behaviour of fibre-reinforced concrete, since flexural tests provide only indirect information on the intrinsic tensile response of the material (Baby et al., 2013).

In the present study, the material parameters previously defined on the basis of the RDP test were used to develop a numerical model of a three-point bending beam test following the standard EN 14651 test arrangement. The EN 14651 method evaluates the behaviour of fibre-reinforced concrete by means of the load–CMOD relationship obtained from a simply supported notched beam subjected to a central point load (EN 14651, 2005).

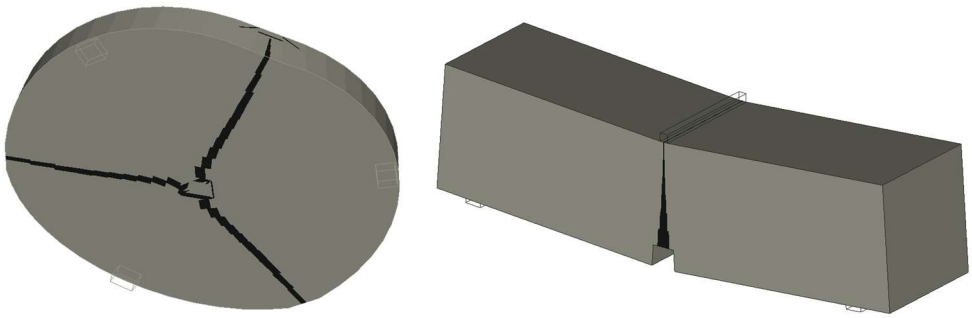


Figure 2: Crack propagation of RDP (left) and EN 14651 beam test (right) models

The aim of the inverse analysis was to determine the material parameter required for further analytical design. For this purpose, the beam test was simulated using the same material parameters that had previously been calibrated from the RDP test. Although the fibre orientation was not modelled explicitly, the material model was derived from tested panels whose performance inherently depends on the actual fibre orientation; therefore, the effect of fibre orientation was included implicitly. The main output parameter of the analysis was the f_{Ftu} value, which can serve as a basis for subsequent analytical design. The f_{Ftu} parameter was determined according to the rigid-plastic material idealization adopted in the fib Model Code 2020 framework, in which the post-cracking tensile behaviour of fibre-reinforced concrete is related to residual strength parameters obtained from bending tests (di Prisco et al., 2013). Figure 2 shows the crack propagation of RDP and beam models.

Accordingly, the load–CMOD curve obtained from the numerical analysis was first used to determine the f_{R3} parameter, and the f_{Ftu} value was then calculated from this result following the *fib* Model Code approach (di Prisco et al., 2013). Finally, the f_{Ftu} values obtained from the inverse analysis were compared with those derived from the experimental beam test results. The results and the corresponding differences are presented in Table 7. This comparison provides an assessment of how accurately the material model calibrated on the basis of the RDP test can reproduce the residual design parameters obtained from the EN 14651 beam test.

Table 7: Mean results of the inverse analysis

Casting method	**Dosage (kg/m^3)**	**Residual flexural strength of the test**	**Residual flexural strength of the FEA**	**Difference**
		$f_{Ftu.test}$ [MPa]	$f_{Ftu.FEA}$ [MPa]	[-]
Sprayed	4 kg/m^3	0.42	0.41	3%
Cast	4 kg/m^3	0.81	0.80	1%
Sprayed	7 kg/m^3	0.85	0.76	10%
Cast	7 kg/m^3	1.76	1.59	9%

For this comparison, the results of those beam tests were used in which the specimens had been cut from large cast or sprayed panels. In this way, it could be ensured that the wall effect did not have a significant influence on the measured response, and that the structural behaviour observed in the panel tests remained consistent with that obtained from the beam specimens. This approach was particularly important for the assessment of sprayed and cast materials, since the specimen preparation method may influence fibre orientation and distribution.

Based on the results summarized in Table 7, it can be concluded that the inverse analysis provided a good estimation of the residual flexural strength in all investigated cases. The

difference between the values derived from the experimental tests and those obtained from the finite element analysis remained limited for all specimen types and fibre dosages. The maximum deviation was 10%, which can be regarded as acceptable, particularly when considering the inherent scatter of fibre-reinforced concrete test results.

A generally good agreement can be observed for both casting methods. At the lower fibre dosage of 4 kg/m^3, the correspondence between the experimental and numerical results was especially close, with deviations of only 3% for the sprayed specimens and 1% for the cast specimens. At the higher dosage of 7 kg/m^3, the differences increased to 10% for the sprayed specimens and 9% for the cast specimens. Although these deviations are still within an acceptable range, they indicate that the accuracy of the inverse analysis slightly decreases with increasing fibre content.

It can also be seen that, in the case of sprayed panels, the differences were slightly higher than those observed for the cast specimens. This tendency may be related to the more pronounced variability in fibre orientation and distribution resulting from the spraying process, which can influence the post-cracking behaviour and, consequently, the residual strength parameters derived from the tests. A similar trend can be identified for the higher fibre dosage, where the discrepancy between test and numerical results became larger for both production methods. Nevertheless, the overall agreement confirms that the inverse analysis procedure is capable of providing a reliable estimate of the f_{Ftu} parameter and can therefore be considered suitable for deriving input values for further analytical design.

A comparison of the numerical and analytical approaches indicates that both methods are capable of providing a satisfactory estimation of the mean f_{Ftu} value. Based on the comparison with the experimental results, the numerical procedure showed the higher overall accuracy, with an average deviation of approximately 6%, whereas the analytical method resulted in an average difference of about 12%. It can further be observed that the closest agreement between the numerical and analytical predictions was obtained for the sprayed specimens with a fibre dosage of 7 kg/m^3. At the same time, the numerical model generally provided more accurate estimates at the lower fibre dosage level, indicating that the predictive capability of the numerical approach was strongest in the less heavily fibre-reinforced mixes. In addition, while the numerical model consistently underestimated the f_{Ftu} value, the analytical method overestimated it in almost all cases, indicating that the numerical inverse analysis provides results on the safe side.

In conclusion, deriving the f_{Ftu} value from panel test results can be particularly useful in the design of shotcrete linings. In many cases, structural verification requires not only the assessment of energy absorption, but also the preparation of normal force–moment interaction diagrams, for which the f_{Ftu} parameter is essential. In this respect, sprayed panel test results may provide a more representative basis for design than traditional beam tests, especially when the beams are cast. Since fibre orientation and distribution in shotcrete are strongly influenced by the spraying process, panel tests produced under realistic application conditions can better reflect the actual structural behaviour. Therefore, the presented methods can provide a more accurate basis for further analytical design.

5 Concluding remarks

The study shows that the selection of the test method has a major influence on the measured post-cracking behaviour of fibre-reinforced concrete, especially for sprayed applications, where fibre orientation and accelerator effects strongly affect the results. The experimental results indicate that round determinate panel testing provides lower scatter and a more representative assessment of sprayed concrete performance than conventional beam testing, particularly when compared with beams affected by wall-induced fibre alignment. The analytical conversion of panel test results into equivalent stress–crack width relationships demonstrated good agreement with beam-based residual strengths, supporting the use of RDP testing as a basis for constitutive characterization and design. The numerical modelling and inverse analysis further confirmed that material parameters calibrated from panel tests can reproduce both panel energy absorption and beam-derived f_{Ftu} values with acceptable accuracy. In conclusion it can be stated that deriving design parameters directly from sprayed panel tests can provide a more reliable and realistic basis for the analytical design of shotcrete linings than relying solely on traditional beam testing.

6 Acknowledgements

The Authors acknowledge the support provided by BarChip Inc. in funding this work, Cooma Sand & Concrete for preparation of the shotcrete mix, Endacom for providing equipment and personnel for spraying of the samples and K&H Geotechnical Services for conducting the tests described in this paper.

7 References

ASTM C1609/C1609M-19, 2019. *Standard Test Method for Flexural Performance of Fiber-Reinforced Concrete (Using Beam With Third-Point Loading)*, ASTM International, West Conshohocken, PA.

ASTM C1550, 2020. *Standard Test Method for Flexural Toughness of Fiber Reinforced Concrete (Using Centrally Loaded Round Panel)*, ASTM International, West Conshohocken, PA.

Baby, F., Graybeal, B., Marchand, P., and Toutlemonde, F., 2013. "UHPFRC tensile behavior characterization: inverse analysis of four-point bending test results," *Materials and Structures*, 46, pp. 1337-1354.

Bernard, E.S., 2002. "Correlations in the behaviour of fibre reinforced shotcrete beam and panel specimens," *Materials and Structures/Matériaux et Constructions*, 35, pp. 156-164.

Bernard, E.S., 2013. "Development of a 1200-mm-Diameter Round Panel Test for Post-Crack Assessment of Fiber-Reinforced Concrete," *Advances in Civil Engineering Materials*, 2(1), ASTM International.

Bernard. E. S., 2020. "Correlations in Performance of Fiber-Reinforced Concrete Assessed Using EN 14651 and Modified ASTM C1609/C1609M-19 Beam Tests". *Advances in Civil Engineering Materials*. 64–80, pp. https://doi.org/10.1520/ACEM20210127

Cavalaro, S.H.P., and Aguado, A., 2015. "Intrinsic scatter of FRC: an alternative philosophy to estimate characteristic values," *Materials and Structures,* 48, pp. 3537–3555.

CEN, 2004. "EN 1992-1-1:2004+A1:2014 Eurocode 2: Design of concrete structures - Part 1-1: General rules and rules for buildings," *European Committee for Standardization*, Brussels, Belgium

Červenka, J., and Papanikolaou, V.K., 2008. "Three dimensional combined fracture-plastic material model for concrete," *International Journal of Plasticity*, 24(12), pp. 2192-2220.

Červenka, V., Jendele, L., and Červenka, J., 2026. "ATENA Program Documentation Part 1." *Cervenka Consulting*, Prague, Czech Republic.

Cugat, V., Cavalaro, S.H.P., Bairán, J.M., and de la Fuente, A., 2020. "Safety format for the flexural design of tunnel fibre reinforced concrete precast segmental linings," *Tunnelling and Underground Space Technology*, 103, 103500.

di Prisco, M., Colombo, M., and Dozio, D., 2013. "Fibre-reinforced concrete in fib Model Code 2010: principles, models and test validation," *Structural Concrete*, 14(4), pp. 342-361.

EN 14651, 2005. *Test method for metallic fibre concrete — Measuring the flexural tensile strength (limit of proportionality (LOP), residual)*, European Committee for Standardization (CEN), Brussels.

fib, 2024. *fib Model Code for Concrete Structures 2020*. fédération internationale du béton (fib), Lausanne.

Galobardes, I.,Salvador, R., Figueiredo, A., Cavalaro, S. & Rueda, A., 2014. "Wet mix sprayed concrete set accelerating admixtures: Comparison between traditional aluminate based accelerators and new formulations of alkali free accelerators." 10.13140/2.1.3097.3447.

ITAtech Activity Group Support, 2015. *ITAtech Design Guidance for Precast Fibre Reinforced Concrete Segments - Draft Report*, ITAtech Report No. 7 / Draft, July 2015.

Jepsen, M.S., Damkilde, L., Löfgren, I., and Berrocal, C., 2018. "Adaptive inverse analysis (AIA) applied and verified on various fiber reinforced concrete composites," *Materials and Structures*, 51, Article 79.

Juhász, K.P., 2013. "Modified fracture energy method for fibre reinforced concrete," in *Fibre Concrete 2013: Technology, Design, Application*, Prague, Czech Republic, 12-13 September 2013, pp. 89-90, Paper p07.

Juhász, K.P., 2020. "Effects of pouring technique on orientation of steel and synthetic macrofibres in fibre-reinforced concrete." *Concrete Structures*, *21*, pp.2-10.

Menétrey, P., Willam, K.J., 1995. "Triaxial Failure Criterion for Concrete and its Generalization," ACI Structural Journal, 92(3), pp. 311-318

Minelli, F., and Plizzari, G.A., 2015. "Derivation of a simplified stress–crack width law for Fiber Reinforced Concrete through round panel tests," *Cement and Concrete Composites*, 58, pp. 33-43

Parmentier, B., Vandewalle, L., Van Rickstal, F., 2008. "Evaluation of the scatter of the postpeak behaviour of fibre reinforced concrete in bending: a step towards reliability," in 7th RILEM International Symposium on Fibre Reinforced Concrete: Design and Applications (BEFIB 2008), Chennai, India, 17-19 September 2008, pp. 133-143

The Concrete Society, 2016. *TR34: Concrete industrial ground floors — a guide to design and construction*, 4th ed., Camberley: The Concrete Society